Motion of auroral ion outflow structures observed with CLUSTER and IMAGE FUV

L. M. Kistler,[1] H. U. Frey,[2] E. Möbius,[1] C. Mouikis,[1] J. M. Quinn,[1] B. Klecker,[3] H. Rème,[4] J. M. Bosqued,[4] I. Dandouras,[4] J. A. Sauvaud,[4] A. M. Di Lellis,[5] V. Formisano,[5] M. F. Marcucci,[5] C. W. Carlson,[2] J. P. McFadden,[2] G. K. Parks,[2] M. McCarthy,[6] A. Korth,[7] L. Eliasson,[8] R. Lundin,[8] G. Paschmann,[3] M. A. Popecki,[1] S. B. Mende,[2] J. D. Winningham,[9] and A. N. Fazakerley[10]

Received 28 August 2001; revised 26 February 2002; accepted 18 March 2002; published 15 August 2002.

[1] During February 2001 the CLUSTER satellites recorded a number of perigee passes through the midnight auroral zone. We concentrate on one pass, on 23 February 2001, when structured outflow was observed. Simultaneous observations of the aurora were available from the FUV instrument on IMAGE. The features in the ion outflow observed by the Cluster Ion Spectrometry (CIS) experiment are compared with the auroral activity. Observations from the multiple CLUSTER spacecraft are used to determine the velocity of the outflow structures. We find a good correspondence between the observed ion outflow and the auroral arcs, with the highest energy outflow corresponding to the brightest arcs. The features at the equatorward edge, which are trapped precipitating ions, are stationary. In addition, the increased velocity structure at the poleward edge is also stationary. However, the bulk of the ion outflow structures, which are observed between these boundaries, are moving equatorward with a velocity of roughly 7 km/s, which corresponds to a velocity of 0.7 km/s at 100 km. One feature is observed moving poleward, at the same time that the auroral arc is expanding poleward. Comparisons with the motion of the auroral arcs and with the convection velocity measured by the EDI instrument on CLUSTER show that the motion of the structures in general agrees with the convective motion of the field lines. *INDEX TERMS:* 2704 Magnetospheric Physics: Auroral phenomena (2407); 2736 Magnetospheric Physics: Magnetosphere/ionosphere interactions; 2431 Ionosphere: Ionosphere/magnetosphere interactions (2736); 2451 Ionosphere: Particle acceleration; *KEYWORDS:* CLUSTER, aurora, ion, outflow

1. Introduction

[2] Ion outflow from the auroral regions particularly during storm times is a significant source of plasma in the magnetosphere [*Chappell*, 1988; *Young et al.*, 1982]. In order to incorporate ion outflow into global magnetospheric models, it is necessary to understand how the outflow depends on the ionospheric and magnetospheric conditions. A number of statistical studies have shown how the outflow depends on position and geomagnetic activity, as characterized by the AE or Kp index [*Kondo et al.*, 1990; *Norqvist et al.*, 1998]. *Yau et al.* [1988] developed an empirical model of the outflow as a function of AE. However, a recent study [*Peterson et al.*, 2002] has shown that the actual outflow can vary by as much as four orders of magnitude from the average value. They conclude that, like the electron precipitation and the visible auroral arcs, the auroral ion outflow structures are also filamentary in nature, and highly variable in space and time, and the outflow must be modeled accordingly.

[3] If the ion outflow intensity were correlated with the visible auroral arcs, the arcs could be used as a proxy for determining the amount of outflow. The ions which are accelerated out of the aurora can be divided into two categories, beams and conics (for a review, see *Andre and Yau* [1997]). Ion beams are generated by parallel electric fields, which at the same time accelerate the auroral electrons downward, and would therefore be expected to correlate with the visible arcs. Ion conics are caused by an acceleration of ions perpendicular to the magnetic field, due to the oscillation of the perpendicular electric field component. The dominant ion heating seems to be

[1]Space Science Center, University of New Hampshire, Durham, New Hampshire, USA.
[2]Space Sciences Laboratory, University of California, Berkeley, California, USA.
[3]Max-Planck-Institut für Extraterrestriche Physik, Garching, Germany.
[4]Centre d'Etude Spatiale des Rayonnements, Toulouse, France.
[5]Istituto di Fisica dello Spazio Interplanetario, Rome, Italy.
[6]Geophysics Program, University of Washington, Seattle, Washington, USA.
[7]Max-Planck-Institut für Aeronomie, Katlenburg-Lindau, Germany.
[8]Swedish Institute of Space Physics, Kiruna, Sweden.
[9]Department of Space Sciences, Southwest Research Institute, San Antonio, Texas, USA.
[10]Mullard Space Science Laboratory, University College London, Surrey, United Kingdom.

0148-0227/02/2001JA005075$09.00

from the broadband waves [*Andre et al.*, 1998]. These waves are correlated with field-aligned fluxes of 10 eV-1 keV electrons, and are not well associated with the downgoing auroral keV electrons. Thus, heating by this mechanisms may not occur on the same field lines as the auroral arcs.

[4] If the outflow is correlated with the arcs, the outflow regions would be expected to move with the arcs when the aurora expands. A number of observations [*Wescott et al.*, 1970; *Kelley et al.*, 1971; *Haerendel*, 1972] have shown that the fast poleward motion of an arc is not accompanied by poleward convection of the plasma, but the regions where the outflow originates could still be moving poleward. *Haerendel et al.* [1993] also showed in some cases with slow moving arcs that the convective motion of the plasma can be different from the arc motion. The ion beams associated with the potential structures which form the arc, would be expected to move with the arcs. Whether the regions of wave heating also move with the arcs or convect with the plasma is not so clear.

[5] Some attempts have been made to correlate the observed ion outflow with the simultaneous auroral emissions. *Yamamoto et al.* [1993] performed a comprehensive study of the ion, electron, and field structures compared with what was observed in the UV auroral structures, using Akebono data at about 10000 km. They found that the discrete arcs correlated well with observations of ion beams, and that there was a region poleward of the discrete arcs where ion conics were observed. *Hirahara et al.* [1998] compared the upward field aligned ion beams and conics observed on Polar with simultaneous observations of the aurora from the UVI instrument during two dusk and one dawn-side pass through the southern aurora. The in-situ ion measurements were made at about 5000 km. They found that ion conic distributions were not correlated with significant auroral emissions, and were often observed at higher latitudes than the auroral forms. The beams were associated with bright discrete auroral signatures, in agreement with *Yamamoto et al.* [1993]. *Wilson et al.* [2001] performed a statistical analysis comparing the outflowing O^+ flux (10–1000 eV) and auroral emissions measured by UVI for time periods close to midnight, during winter, solar minimum conditions. They found that auroral emissions always correlate with high O^+ outflow, with the peak correlation occurring with a delay of about 5 min between emission and O^+ observation. However, there are also periods of O^+ outflow which do not have an associated emission. They did not divide up their O^+ outflow into "beams" or "conics".

[6] The CLUSTER mission in combination with global auroral observations by IMAGE-FUV gives us an opportunity to compare both the occurrence of ion outflow with the auroral emission, and the motion of the ion outflow location with the motion of the auroral structures. During the 23 February 2001 event, the FUV camera on IMAGE observed the northern aurora. By comparing the times at which the same outflow structures are observed on the different CLUSTER satellites, we are able to determine the velocity of the structures. We compare the intensity and velocity of the ion outflow structures observed by the CIS instrument on the CLUSTER satellites with the emissions and location of the aurora at the same time and with the convection velocity measured simultaneously on the CLUSTER satellites by the EDI instrument.

2. Instrumentation

[7] The CLUSTER satellites are in highly elliptical polar orbits, with apogee of 19.8 Re and a perigee of 4.0 Re. The line of apsides is in the ecliptic plane. The data shown here are mainly from the Composition and Distribution Function (CODIF) analyzer, which is part of the Cluster Ion Spectrometry (CIS) package. CODIF measures the 3-dimensional distribution functions of the major ion species in the magnetosphere, magnetosheath, and solar wind over the energy per charge range 20–40000 eV/e. It is a combination of a top-hat electrostatic analyzer followed by a post-acceleration of 15 kV and a time-of-flight measurement. It can resolve the major ion species, H^+, He^{++}, He^+ and O^+. The electrostatic analyzer is divided into two halves, with geometric factors different by a factor of 100. Only one half operates at a time, giving a 180^o instantaneous field of view divided into 8 sectors of 22.5^o each. The electrostatic analyzer sweeps through the full energy range 32 times per spin, so that the full distribution is obtained in one spin. A detailed description of the instrument is given by *Rème et al.* [2001].

[8] An onboard processor collects the event data from the sensor and classifies each event by mass, energy, and angle. It then bins the data and creates data products which consist of 3-dimensional (3D) distributions, a mass spectrum, and moments of the distribution. 3D distribution products are available for each of the 4 major species, H^+, O^+, He^{++}, and He^+, with either 16 or 32 energy bins, and 88 or 24 angular bins. The combination of products obtained at any time and their time resolution depends on the telemetry rate and the expected count rates for the particular species in the measurement region.

[9] Auroral images are obtained using one of the three far ultra violet imaging instruments (FUV) on the IMAGE spacecraft, the Wideband Imaging Camera (WIC), which observes emissions of the molecular nitrogen LBH-band and some atomic nitrogen lines in a passband between 140 and 180 nm [*Mende et al.*, 2000]. These emissions are primarily excited by electron precipitation, though energetic protons may contribute significantly in certain regions of the auroral oval [*Frey et al.*, 2001]. WIC has a field of view of 17.2× 17.2 degrees which allows for a good observation of the full northern auroral oval for about 9 hours during every 14 hours orbit. An image is obtained every 122 seconds, which is the spin period of the spacecraft. During the time of this investigation IMAGE was descending from apogee, and the instantaneous geocentric distance translates into a pixel size of about 50 km at ionospheric altitude. All images shown here were mapped into a geomagnetic MLT-latitude grid.

[10] The Electron Drift Instrument (EDI) on CLUSTER measures the local convection velocity by tracking an electron beam emitted from the spacecraft. It is described in detail by *Paschmann et al.* [1997]. The electron measure-

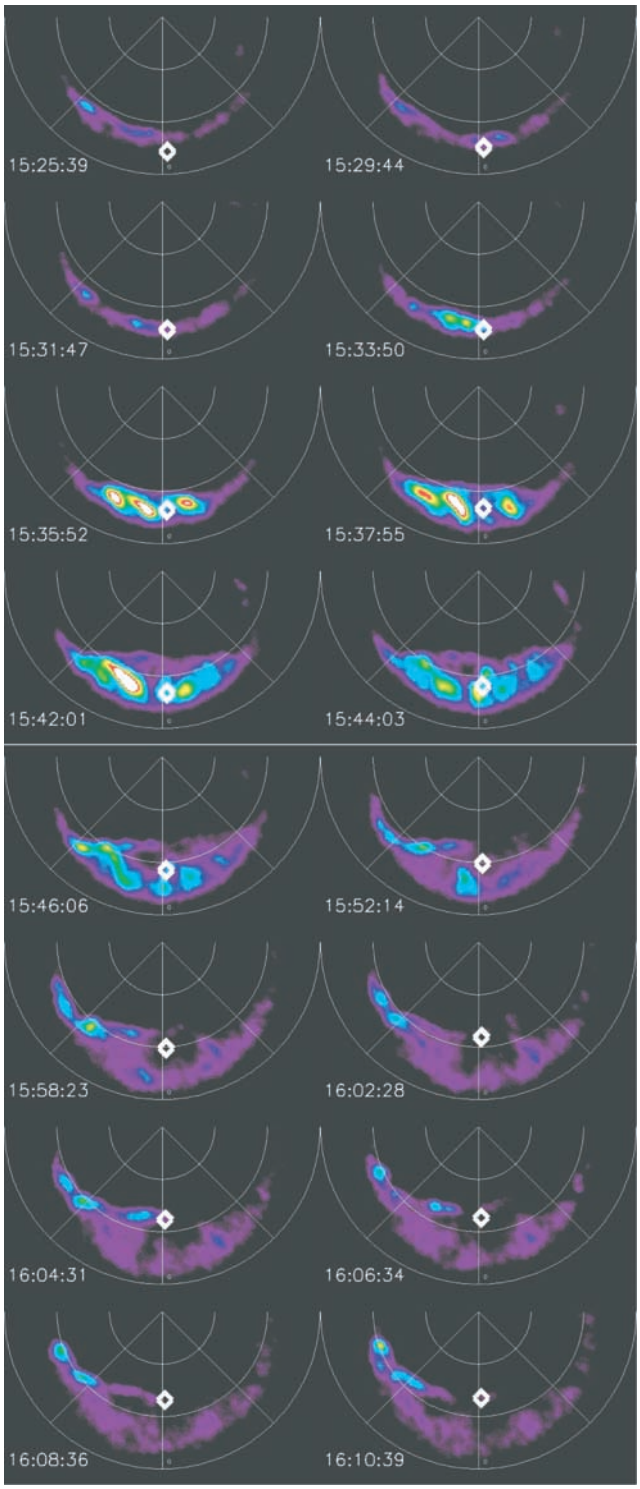

Figure 1. Sequence of auroral images from the FUV camera on IMAGE from 15:25–16:10 on 23 February 2001 mapped into magnetic coordinates. The locations of the foot points of the magnetic field lines corresponding to CLUSTER satellites 1, 3 and 4 are shown with white diamonds. S/C 1 is always the most poleward, and S/C 4 is the most equatorward.

ments are obtained with the Plasma Electron and Current Experiment (PEACE). In this paper, data from the pitch angle distributions (PAD) mode is used which gives a complete PAD every four seconds with 15° resolution. PEACE is described by *Johnstone et al.* [1997].

3. Observations

[11] On 23 February 2001 the CLUSTER satellites recorded a full pass through perigee, measuring first the southern auroral zone and then the northern auroral zone at approximately midnight local time. The day was fairly active, with multiple substorms occurring. Substorm onsets were identified at 12:40 and 15:35 UT, from increases in AE and particle injections signatures at geosynchronous orbit. Some aspects of this event were discussed by *Rème et al.* [2001]. In this paper, we concentrate on the pass through the northern auroral oval, from approximately 15:15–16:15 UT, which occurred during the 15:35 substorm. Figure 1 shows a series of auroral images in magnetic coordinates covering from 15:25–16:10 UT. The foot points of CLUSTER spacecraft 1,3, and 4 are shown with three overlapping white diamonds, centered on the spacecraft locations. S/C 1 is always the furthest poleward, and S/C 4 the furthest equatorward. From 15:25–15:31 UT, there is a stable auroral arc that crosses midnight at about 65° magnetic latitude. The CLUSTER spacecraft move through this structure at about 15:29 UT. At 15:33 UT the aurora brightens, and then expands. The CLUSTER spacecraft remain in the bright part of the arc until after 15:44 UT. From 15:48–15:58 UT, the aurora maintains a double-arc structure, with CLUSTER mainly in the darker region between the two arcs. At 15:58 UT, CLUSTER begins to enter the eastward edge of the poleward arc. At 16:04 UT, that arc brightens over the CLUSTER spacecraft. The arc then fades slightly, and CLUSTER moves into the dark polar cap.

[12] Figure 2 shows a plot of the plasma data on S/C 1 as the spacecraft moves from the radiation belt and ring current region through the northern auroral zone at about 4.5 Re geocentric distance. The panels, from top to bottom, show the H^+ energy spectra, three pitch angle spectrograms covering the energy ranges 3–10 keV, 0.3–3 keV, and 0.03–.3 keV, the same sequence of panels for O^+, and finally energy spectra of downgoing electrons and electrons perpendicular to the magnetic field, from the PEACE instrument. Time periods with significant flux in the downgoing electron spectrum indicate regions which contain a complex mixture of upgoing and downgoing beams and conics. Below each panel is a colored bar which indicates the different regions, as discussed below. There is significant ion outflow in both H^+ and O^+. The outflow is highly structured, changing in both energy and flux magnitude over the course of the event. Until 15:30, the ion distributions are predominantly symmetric about 90° pitch angle, with equal fluxes upgoing and downgoing along the field line. We interpret this to be a trapped, mirroring population. The loss cone in this region is too small to be observed given the 22.5° angular resolution of the data. From 15:27–15:29 UT, there is an enhancement of low energy (<1 keV) O^+ and H^+, which is predominantly perpendicular to the field for O^+ (8th panel) and predominantly field aligned but

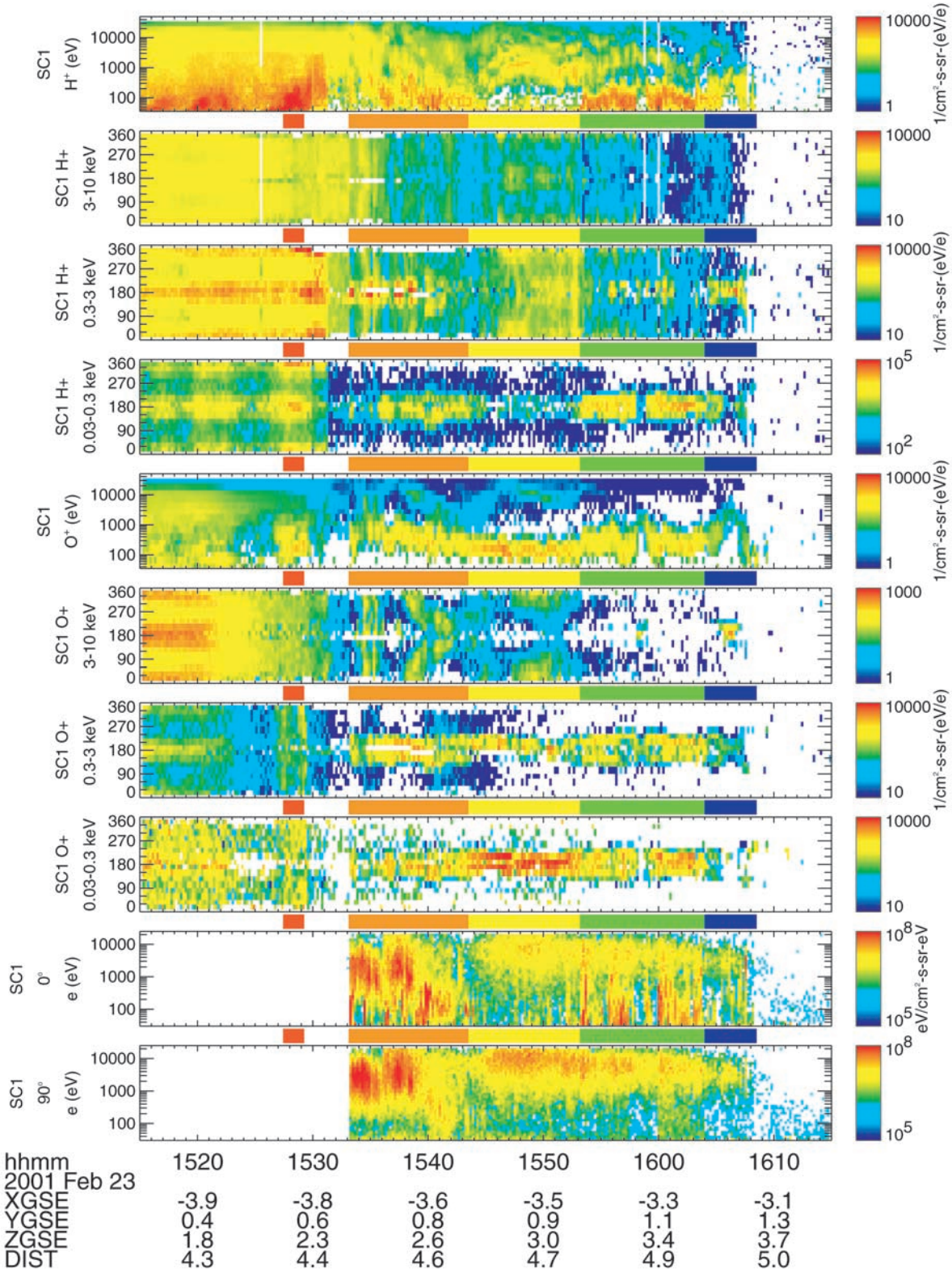
SC1 H+ (eV)
SC1 H+ 3-10 keV
SC1 H+ 0.3-3 keV
SC1 H+ 0.03-0.3 keV
SC1 O+ (eV)
SC1 O+ 3-10 keV
SC1 O+ 0.3-3 keV
SC1 O+ 0.03-0.3 keV
SC1 0° e (eV)
SC1 90° e (eV)
1/cm²-s-sr-(eV/e)
eV/cm²-s-sr-eV
hhmm
2001 Feb 23
XGSE
YGSE
ZGSE
DIST
1520 1530 1540 1550 1600 1610
-3.9 -3.8 -3.6 -3.5 -3.3 -3.1
0.4 0.6 0.8 0.9 1.1 1.3
1.8 2.3 2.6 3.0 3.4 3.7
4.3 4.4 4.6 4.7 4.9 5.0

symmetric for H^+ (4th panel). This is indicated with the red bar below the spectrogram. From 15:33–16:08 UT there is a mixture of a low energy outflowing population, peaked at 180° pitch angle, and a higher energy population originating in the plasma sheet, which is sometimes downgoing, and sometimes symmetric/trapped. From 15:33 to 15:43 UT (orange bar), outflow is observed for both species in the energy range 0.03–3 keV. There are accompanied by energetic electrons with energies up to 10 keV. Field-aligned beams and conics are observed in the electrons from 15:37 to 15:43. At 15:43 UT, the H^+ outflow flux decreases, and the O^+ outflow energy decreases. The low energy O^+ outflow continues without much change until 15:53 UT, as indicated by the yellow bar. During this time, there is an energetic electron population observed at all pitch angles, most likely originating in the plasma sheet. At 15:53 UT, the O^+ outflow increases in energy, there is an increase in the low energy H^+ outflow, and low-energy field-aligned electrons are observed. This lasts until 16:04 UT (green bar). Finally there is an increase in the energy of the ion outflow up to almost 10 keV, followed by a decrease, observed in both H^+ and O^+ (purple bar).

[13] In a rough visual comparison, we can see how the auroral features from Figure 1 compare with the ion outflow from Figure 2. The passage of the spacecraft through the stable arc at 15:29:44 UT corresponds to the enhancement of trapped H^+ and O^+ observed from ~15:27 to 15:29 (red bar). This is most clearly observed in the O^+ energy spectrogram (5th panel). The onset of strong ion outflow (orange bar) corresponds closely to the brightening of the arc at 15:33. As the spacecraft moves into the darker auroral regions, the energy of the outflow decreases to ~100 eV for O^+ and to less than 40 eV for H^+ (yellow bar), and there are no field-aligned electrons. The increase in the energy of the outflow at 15:53 (green bar) and onset of field-aligned electrons occurs as the spacecraft enter the dim eastward edge of the poleward arc. Finally, the large energy increase in the ion outflow (purple bar) corresponds with moving through the poleward arc. Thus the higher energy outflow and field-aligned electrons correlate with the observations of arcs, while the lower energy outflow is found in the dark aurora between the arcs.

[14] The structured nature of the outflow observations allows us to identify specific features. We can then determine when these features are observed on the different spacecraft and use them to determine the motion of the ion outflow structures with time. The motion can then be compared to the motion of the imaged aurora and to convective motion. In general, the outflowing O^+ population is better separated in energy from the higher energy precipitating plasma sheet population than is the outflowing H^+ population. For example, the 0.3–3 keV pitch angle distribution (3rd panel) for H^+ shows a large isotropic component combined with the bursts of outflow. The 0.3–3 keV pitch angle distribution for O^+ (7th panel), on the other hand, is almost completely ion outflow. This makes it easier to use the O^+ to isolate features in the outflow that we can track from one spacecraft to the next. For that reason, much of our analysis of motion concentrates on the O^+ data.

[15] Figure 3 shows the energy-time spectrograms of H^+ and O^+ from three of the CLUSTER spacecraft, S/C 1, S/C 3, and S/C 4 for the time period 15:15–16:15 UT. The spacecraft are traveling north in approximately the X–Z plane, with S/C 1 leading and S/C 4 trailing. Many of the same features are observed on all three spacecraft. In the O^+ spectra, for example (panels 4,5,6), the enhancement in the 100 eV O^+ that begins at 15:27:30 on S/C 1, is subsequently observed at S/C 3 beginning at 15:28:53 and S/C 4 at 15:31:26, as shown by the red bar below each spectrogram. After this, the sequence of outflow observed first at S/C 1 can be observed at S/C 3, and finally at S/C 4. There is one feature which clearly has the reverse order. At 15:42, there is a strong increase in the energy of O^+ observed on S/C 4 (black bar on last panel). A smaller increase is observed later on S/C 3 (black bar), and is not observed at all on S/C 1. This indicates a moving structure that is overtaking the spacecraft, and not reaching S/C 1.

[16] To determine the velocity of the outflow structures and the trapped structures perpendicular to the magnetic field, we need to compare the observed delay between the spacecraft with the delay expected from purely spatial motion. To do this quantitatively, we have calculated density and velocity moments of H^+ and O^+ over the energy range of the outflow distribution, identified features which could be tracked between spacecraft, and then recorded the times at which the features are observed.

[17] Figure 4 shows the H^+ (thin line) and O^+ (thick line) density and velocity moments from the three spacecraft. The total velocity, v, is shown, but this velocity is dominated by the velocity along the magnetic field. The O^+ moments are integrated over the energy range 30–3000 eV, while the proton moments are integrated over 30–300 eV. The reduced energy range for H^+ was used so that the moments would characterize the outflowing portion of the population. We have identified 8 features, labeled "a" through "c" and "e" through "i", that could be observed on all three spacecraft to track the motion. Two of the features (a and c), have both an identified start and stop time. In addition, we identified one feature, labeled "d", the increase in O^+ energy noted in Figure 3, that was only observed on 2 spacecraft. These features, and the times at which they are observed, are given in Table 1. Each of the features is marked in Figure 4 with a bar below the feature, and a letter indicating which feature listed in Table 1 it corresponds to. The final two features, h and i, occur almost simultaneously on S/C 1. Feature h is a minimum observed in the H^+ and O^+ density, and feature i is the peak velocity of the O^+

Figure 2. (opposite) Plasma composition data from the CIS1 and PEACE instruments on CLUSTER S/C 1 for the time period 15:15–16:15 on 23 February 2001. During this time, the spacecraft is at 4 Re, and traveling northward in the X-Z plane. The panels, from top to bottom, show the H^+ differential flux as a function of energy, H^+ pitch angle distributions, for energy ranges 3–10 keV, 0.3–3 keV and 0.03–.3 keV, O^+ differential flux as a function of energy, O^+ pitch angle distributions for the same energy ranges, and differential flux as a function of energy for downgoing electrons and electrons perpendicular to the magnetic field. The colored bar below each panel delineates the different regions, as discussed in the text.

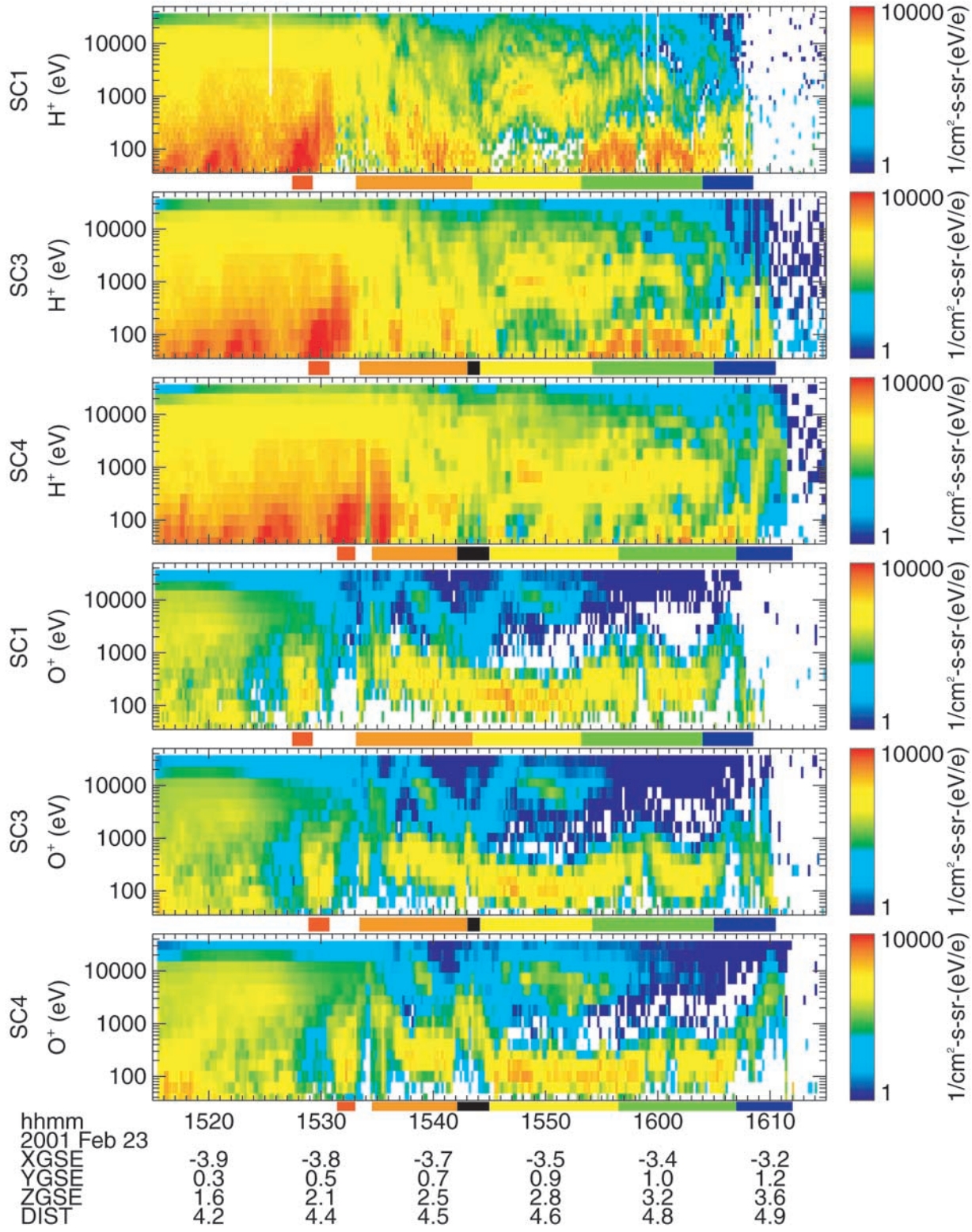

Figure 3. Differential flux vs. energy for the time period 15:15–16:15. From top to bottom, the panels show H^+ for S/C 1, 3 and 4, followed by O^+ for S/C 1, 3, and 4. The colored bar below each panel show when different regions are crossed for each spacecraft, as discussed in the text.

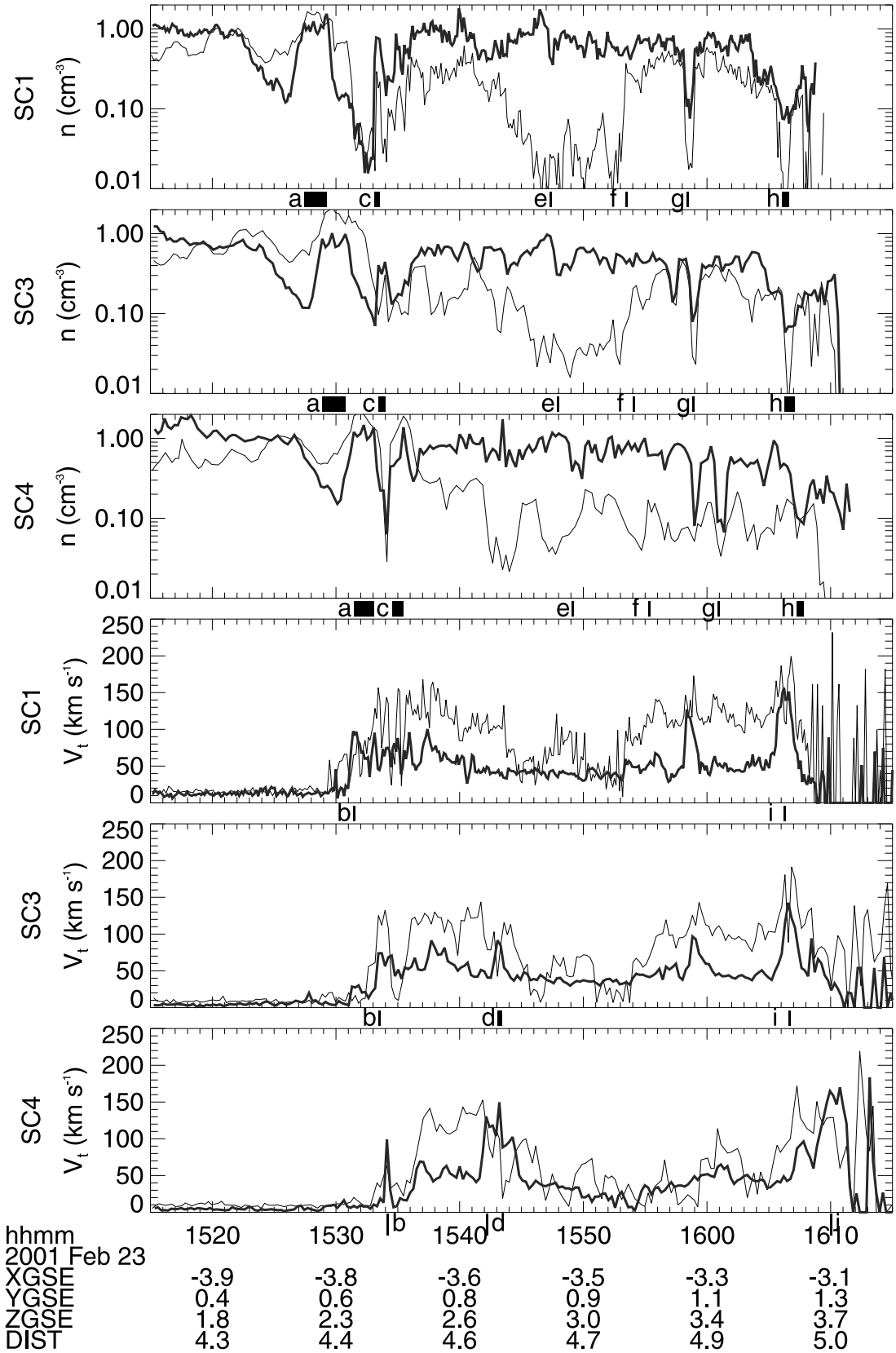

Figure 4. H^+ moments calculated from 30–300 eV (thin line) and O^+ moments calculated for 30–3000 eV (thick line). These energy ranges cover the main outflow energies. The panels, from top to bottom, show density from S/C 1, 3, and 4 and total velocity from S/C 1, 3, and 4. The events shown by the bars below each panel are listed in Table 1.

Table 1. Descriptions, Times, and Velocities for Each of the Features Indicated in Figure 4

Feature	Description	S/C 1 Time	S/C 3 Time	S/C 4 Time	V-Perp SC 1−4, km/s	V-Perp SC 3−4, km/s	V at 100 km SC 1−4, km/s	V at 100 km SC 3−4, km/s
a1	O+ density enhancement start (trapped/bi-directional)	15:27:26	15:28:53	15:31:26	−1.33±0.07	0.10±−0.01	−0.12	−0.03
a2	O+ density enhancement end (trapped/bi-directional)	15:29:15	15:30:45	15:33:03	−1.52±0.08	−0.43±0.05	−0.15	−0.07
b	Start of O+ velocity enhancement (outflow)	15:31:23	15:33:26	15:34:07	−3.69±0.27	−12.54±5.77	−0.35	−1.10
c1	O+ density enhancement— first point after minimum	15:33:07	15:33:26	15:34:33	−11.24±1.60	−5.93±1.50	−0.97	−0.54
c2	O+ density enhancement — last point before fall-off	15:33:31	15:33:58	15:35:27	−7.24±0.76	−3.46±0.64	−0.63	−0.33
d	Increase in O+ velocity		15:43:03	15:42:08		17.88 5.68		1.56
e	Low energy (<200 ev) O+ min after peak	15:47:16	15:47:52	15:49:05	−7.64±0.85	−6.15±1.42	−0.71	−0.55
f	H+ low energy enhancement onset	15:53:26	15:54:00	15:55:14	−7.86±0.88	−6.08±1.38	−0.71	−0.56
g	H+/O+ density minimum in lowE enhancement	15:58:21	15:58:49	16:00:51	−4.20±0.34	−1.88±0.25	−0.41	−0.20
h	O+ density minimum center	16:06:21	16:06:42	16:07:32	−13.37±2.33	−10.29±3.67	−1.16	−1.05
I	Peak in outflow velocity	16:06:13	16:06:34	16:09:56	−1.34±0.07	0.31±−0.02	−0.12	0.02

outflow. Because the time of the two features is significantly different on S/C 4, the two features give very different velocities for the structures.

[18] Figure 5 shows the latitude and longitude, in GM coordinates, of the foot point of the spacecraft location at the time that each of the nine features are observed. For each feature, the same symbol is used for all three spacecraft. If the structures that the spacecraft were moving through were stationary and ordered by L-shell, the spacecraft would observe them at approximately the same latitude. The first feature (features a1 and a2) and the final increase in energy (feature i) are observed with latitudinal differences of only a quarter of a degree. For features b through g, however, a difference in latitude of about 0.5 to 0.75 degrees is observed by the three spacecraft. We have used the time delay and the separation between S/C 1 and 4 and S/C 3 and 4 perpendicular to the magnetic field to calculate the perpendicular velocity of the structure at the spacecraft location. Because the spacecraft are not well separated in Y, and are moving mainly in the X and Z plane (corresponding to latitude) we can only determine the structure velocity in this plane. Table 1 gives the results. The error column indicates the error that results from the time resolution of the O^+ data. During this time, the O^+ distributions are measured every 8 s on S/C 1 and every 16 s on S/C 3 and 4, so an error in the time of ± 16 s is assumed for the S/C 3−4 velocity, and ± 12 s for the S/C 1−4 velocity. This is really a lower limit, since there may be additional errors in determining the feature times to within one data point. In general, the errors on the SC 1−4 velocities are smaller, because the time between the observed features is larger. For the features a1, a2, and i, the S-C 1−4 time difference would correspond to a velocity of about 1.4 km/s. Features b and g give velocities of about 4 km/s, and features c3, e and *F* give velocities of about 7.5 km/s. All these velocities are in the equatorward direction. Feature d gives a poleward motion of 17 km/s. In order to determine the corresponding velocity at ionospheric altitudes, we have traced the field lines to 100 km altitude in GSM coordinates using the NASA SSCWeb tracing tool, and then determined the latitudinal velocity. The final two columns of Table 1 contain these results.

[19] In order to compare the ion outflow motion with the changes in the aurora, we have re-plotted the auroral image data in a keogram format. Figure 6 shows the auroral emissions as a function of time at local midnight, the local time at which the spacecraft passed through the aurora. The black line gives the spacecraft latitude of S/C 3. The black arrows on Figure 6a show the velocities determined by tracking the outflow structures between the spacecraft. In this latitude-time plot, the velocity is given by the slope of the arrow. Because the arrows are drawn for equal time segments (the length in X) the length of the arrow in Y is also proportional to the velocity. When the spacecraft is in the initial stable arc at 15:29 UT, the velocity is small (horizontal arrow). When the spacecraft enters the brighter regions, the equatorward velocity follows the contours of the auroral images. The poleward moving structure, which is observed on the two most equatorward spacecraft, corresponds to a time when the spacecraft are on the edge of a brightening expanding structure. S/C 1 must have been just poleward of this enhancement and thus missed it. After that, there are not many auroral structures to compare the velocities with, until the poleward arc, which is stable. At the poleward arc, we observed the density feature, which is convecting equatorward, and the velocity feature which is relatively stationary. This may indicate that the potential structure is stationary, while the plasma is still convecting.

[20] Finally, we compare the observed velocity with the convection velocity observed at the same time with the Electron Drift Instrument (EDI) for this time period. EDI turned on at about 15:40 UT. Figure 6b shows the same keogram with the EDI convection velocity measurements, averaged over 30s intervals, also in the X−Z plane, indicated with white arrows. The convection velocities observed during the bright aurora also follow the equatorward motion of the auroral structure. At 15:43 UT, when the outflow structure was observed to move poleward, the convection velocity is also poleward. Then the convection turns equatorward again, as did the motion of the outflow structures.

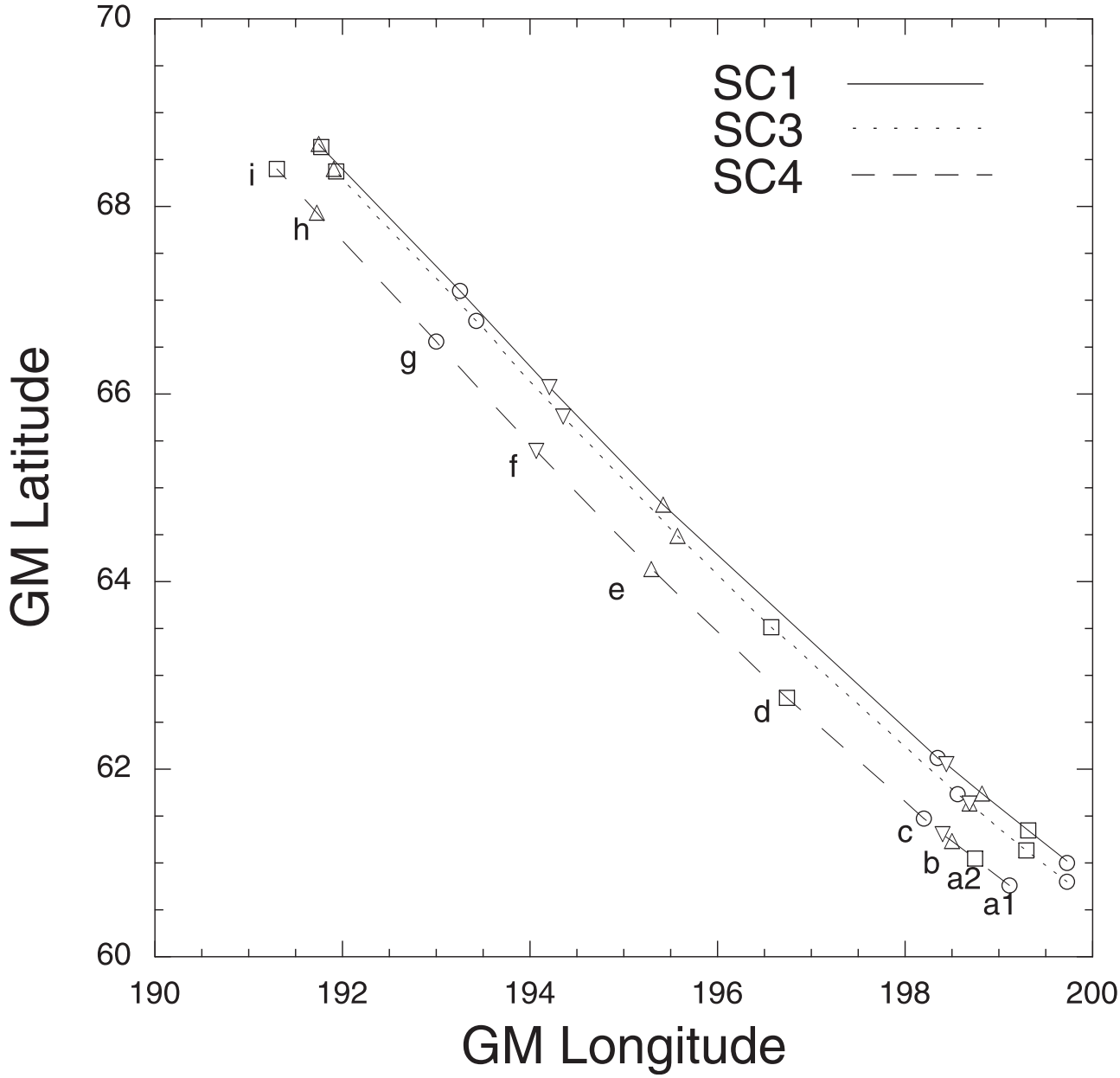

Figure 5. Location of the foot point of the magnetic field lines at the CLUSTER locations at 100 km altitude in GM coordinates for each of the 9 features listed in Table 1. For each feature, the same symbol is used for all three spacecraft.

After 15:52 UT, the convection velocity is highly variable, but not inconsistent with the velocities of the ion outflow structures.

4. Discussion and Conclusions

[21] We have used one example of a CLUSTER pass through the auroral regions to compare the ion outflow with the simultaneously observed auroral emissions and determined the motion of the ion outflow structures. We see a reasonable correspondence between the observed auroral structures and the energy of the outflow. The more intense structures correspond to higher energy outflow. Because of the high altitude of the CLUSTER spacecraft, we are not able to test whether the emissions correspond to ion beams, while the conics correspond to outflow with no emission, as was observed by *Hirahara et al.* [1998] and *Yamamoto et al.* [1993].

[22] By tracking features observed in the ion outflow, we were able to determine whether the region of ion outflow is stationary or moving. There were some structures, both at the equatorward and the poleward edge of the auroral zone, which were stationary during the 3–4 min that it takes for the spacecraft to pass over them. On the equatorward edge was a trapped ion structure, and on the poleward edge was a structure with increasing, then decreasing velocity. The ion outflow structures between these two regions were moving mainly equatorward at about 7 km/s, corresponding to a

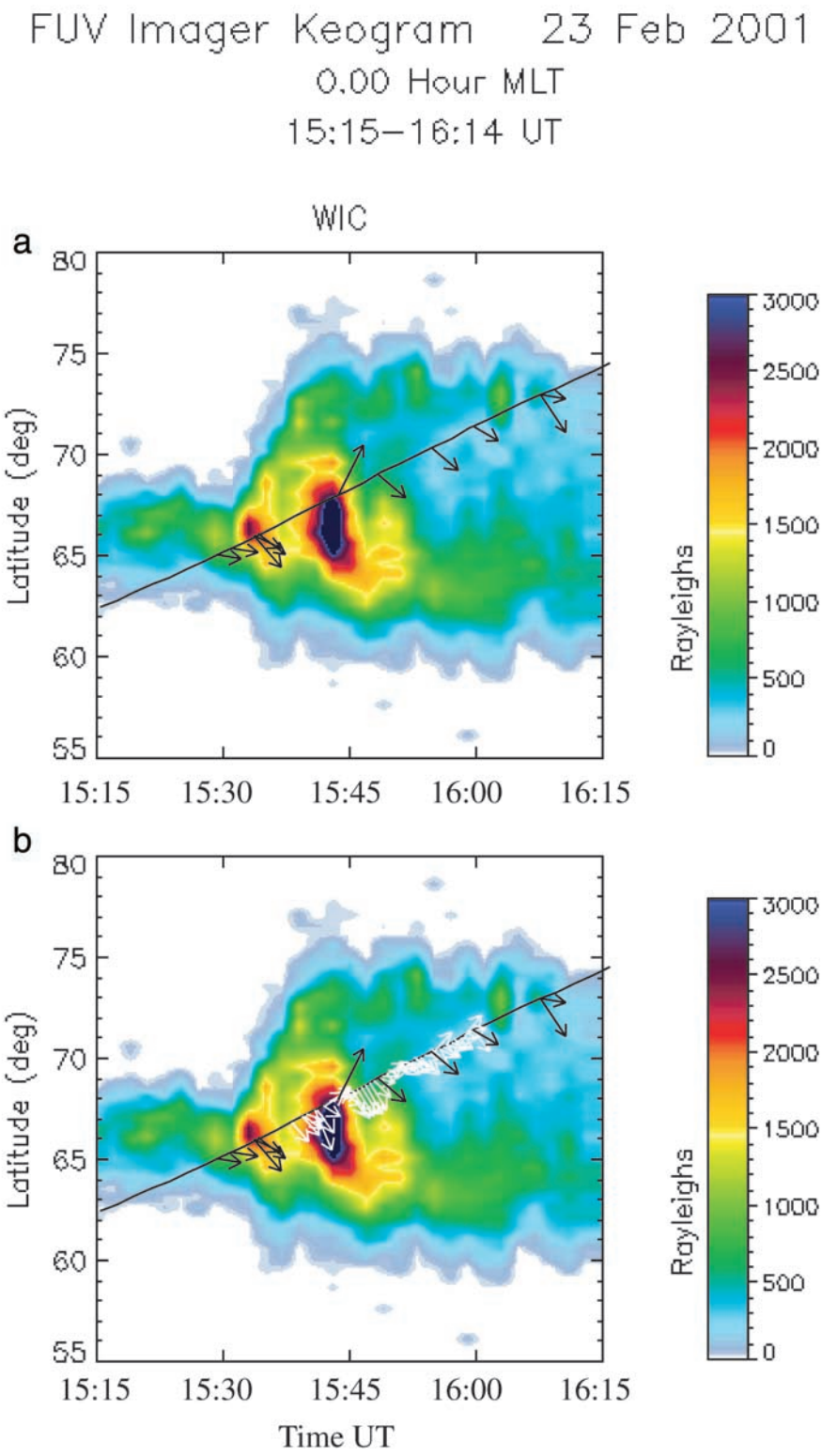

Figure 6. A Keogram showing the auroral emissions as a function of time at midnight MLT from the FUV camera on IMAGE, from 15:15–16:15. The track of the CLUSTER S/C 3 is given by the solid black line. In panel a, the slopes of the black arrows give the velocities of the ion outflow structures. In panel b, the same black arrows are shown, and in addition, the slopes of the white arrows give the convection velocities determined from the EDI instrument on CLUSTER.

velocity in the ionosphere of about 0.7 km/s, with one exception which moved rapidly poleward at 17 km/s (corresponding to 1.5 km/s at 100 km).

[23] The question of whether the motion of the ion outflow regions follows the fast poleward motion of an arc, or follows the plasma convection is left somewhat ambiguous in this case. In general, the motion of the ion outflow structures was found to be consistent with the locally observed convective motion, but the structures also followed the contours of the auroral arc motion. Although the overall arc structure expanded poleward during this event, we only observed one poleward moving ion outflow structure. That time period did correspond with a time when the CLUSTER spacecraft mapped to the poleward edge of an expanding structure, but it also occurred during a time when the convection was poleward. Thus we cannot definitely state from this one case that the outflow follows convection motion, and not arc motion.

[24] The CLUSTER satellites have allowed us, for the first time, to measure the spatial and temporal coherence and the velocity of the structured ion outflow observed in the nightside auroral region during a substorm. We find that many of large–scale outflow structures are coherent over the 3–4 min timescales that it takes for the spacecraft to pass through them. The outflow correlates well with observed auroral arcs, with brighter arcs corresponding to higher energy outflow. The outflow structures are moving with velocities consistent with the convection velocity. However, in this case the convective motion is not substantially different from the apparent motion of the auroral arcs.

[25] **Acknowledgments.** We are grateful to the many engineers and scientists from UNH, MPE, CESR, MPAe, IFSI, IRF, U of Bern, UCB and UW who made the development of the CIS instrument possible. Development of the CIS instrument in the US and this work were supported by NASA contract NAS5–30613 and Grant NAG5-10131. CIS was supported in Germany by ESA under grant 1501073-2400 and by DLR under grants 50OC8906 and 50OC0102.

[26] Michel Blanc thanks Masa Hirahara and another referee for their assistance in evaluating this paper.

References

Andre, M., and A. W. Yau, Theories and observations of ion energization and outflow in the high latitude magnetosphere, *Space Sci. Rev.*, *80*, 24–28, 1997.

Andre, M., P. Norqvist, L. Andersson, L. Eliasson, A. I. Eriksson, L. Blomberg, E. R. Erlandson, and J. Waldemark, Ion energization mechanisms at 1700 km in the auroral region, *J. Geophys. Res.*, *103*, 4199–4222, 1998.

Chappell, C. R., The terrestrial plasma source: A new perspective in solar–terrestrial processes from Dynamics Explorer, *Rev. Geophys.*, *26*, 229–248, 1988.

Frey, H. U., S. B. Mende, C. W. Carlson, J.-C. Gérard, B. Hubert, J. Spann, R. Gladstone, and T. J. Immel, The electron and proton aurora as seen by IMAGE-FUV and FAST, *Geophys. Res. Lett.*, *28*, 1135–1138, 2001.

Haerendel, G., Plasma drifts in the auroral ionosphere derived from barium releases, in *Earth's Magnetospheric Processes*, edited by B. M. McCormac, pp. 246–257, D. Reidel, Norwell, Mass., 1972.

Haerendel, G., S. Buchert, C. LaHoz, B. Raff, and E. Rieger, On the proper motion of auroral arcs, *J. Geophys. Res.*, *98*, 6087–6099, 1993.

Hirahara, M., et al., Relationship of topside ionospheric ion outflows to auroral forms and precipitation, plasma waves, and convection observed by Polar, *J. Geophys. Res.*, *103*, 17,391–17,410, 1998.

Johnstone, A. D., et al., PEACE: A plasma electron and current experiment, *Space Sci. Rev.*, *79*, 351–398, 1997.

Kelley, M. C., J. A. Starr, and F. S. Mozer, Relationship between magnetospheric electric fields and motion of auroral forms, *J. Geophys. Res.*, *76*, 5269–5277, 1971.

Kondo, T., B. A. Whalen, A. W. Yau, and W. K. Peterson, Statistical analysis of upflowing ion beam and conic distributions at DE-1 altitudes, *J. Geophys. Res.*, *95*, 12,091–12,102, 1990.

Mende, S. B., et al., Far ultraviolet imaging from the IMAGE spacecraft, *Space Sci. Rev.*, *91*, 243–318, 2000.

Norqvist, P., M. Andre, and M. Tyrland, A statistical study of ion energization mechanisms in the auroral region, *J. Geophys. Res.*, *103*, 23,459–23,473, 1998.

Paschmann, G., et al., The Electron Drift Instrument for Cluster, *Space Sci. Rev.*, *79*, 233–269, 1997.

Peterson, W. K., H. L. Collin, M. Boehm, A. W. Yau, C. Cully, and G. Lu, Spatial/temporal coherence of ionospheric outflow on January 9–12, 1997, *J. Atmos. Sol. Terr. Phys.*, in press, 2002.

Rème, H., et al., First multispacecraft ion measurements in and near the Earth's magnetosphere with the identical CLUSTER Ion Spectrometry (CIS) experiment, *Ann. Geophys.*, *19*, 1303–1354, 2001.

Wescott, E. M., J. D. Stolarik, and J. P. Heppner, Auroral and polar cap electric fields from barium releases, in *Particles and Fields in the Magnetosphere*, edited by B. M. McCormac, pp. 229–238, D. Reidel, Norwell, Mass., 1970.

Wilson, G. R., D. M. Ober, G. A. Germany, and E. J. Lund, The relationship between suprathermal heavy ion outflow and auroral electron energy deposition: Polar/UVI and FAST, *J. Geophys. Res.*, *106*, 18,981–18,994, 2001.

Yamamoto, T., E. Kaneda, H. Hayakawa, T. Mukai, A. Matsuoka, S. Machida, H. Fukunish, N. Kaya, K. Tsuruda, and A. Nishida, Meridional structures of electric potentials relevant to premidnight discrete auroras: A case study from akebono measurements, *J. Geophys. Res.*, *98*, 11,135–11,151, 1993.

Yau, A. W., W. K. Peterson, and E. G. Shelley, Quantitative parameterization of energetic ionospheric ion outflow, in *Modeling Magnetospheric Plasma, Geophys. Monogr. Ser.*, vol. 44, edited by T. E. Moore and J. H. Waite Jr., pp. 211–217, AGU, Washington, D. C., 1988.

Young, D. T., H. Balsiger, and J. Geiss, Correlations of magnetospheric ion composition with geomagnetic and solar activity, *J. Geophys. Res.*, *87*, 9077–9096, 1982.

J. M. Bosqued, I. Dandouras, H. Rème, and J. A. Sauvaud, Centre d'Etude Spatiale des Rayonnements, 9 Avenue Colonel-Roche, BP 4346, 31029 Toulouse, France.

C. W. Carlson, H. U. Frey, J. P. McFadden, S. B. Mende, and G. K. Parks, Space Sciences Laboratory, University of California, Grizzly Peak Boulevard at Centennial Drive, Berkeley, CA 94720, USA.

A. M. Di Lellis, V. Formisano, and M. F. Marcucci, Istituto di Fisica dello Spazio Interplanetario, Via del Fosso del Cavaliere, 100, 00133 Rome, Italy.

L. Eliasson and R. Lundin, Swedish Institute of Space Physics, P.O. Box 812, S-981 28 Kiruna, Sweden.

A. N. Fazakerley, Mullard Space Science Laboratory, University College London, Surrey RH5 6NT, UK.

L. M. Kistler, E. Möbius, C. Mouikis, M. A. Popecki, and J. M. Quinn, Space Science Center, University of New Hampshire, 410 Morse Hall, Durham, NH 03824, USA. (lynn.kistler@unh.edu)

B. Klecker and G. Paschmann, Max-Planck-Institut für Extraterrestriche Physik, Karl-Schwarzschild Strasse 1, Postfach 1312, D-85740 Garching bei München, Germany.

A. Korth, Max-Planck-Institut für Aeronomie, Max-Planck Strasse 2, Postfach 20, D-37191 Katlenburg-Lindau, Germany.

M. McCarthy, Geophysics Program, University of Washington, ATG Building, Box 351650, Room 202, Seattle, WA 98195, USA.

J. D. Winningham, Department of Space Sciences, Southwest Research Institute, 6220 Culebra Road, PO Drawer 28510, San Antonio, TX 78284, USA.